Purdue University
Purdue e-Pubs

Weldon School of Biomedical Engineering Faculty Publications

Weldon School of Biomedical Engineering

2012

Optimizing Electrode Placement for Hemodynamic Benefit in Cardiac Resynchronization Therapy

Charles F. Babbs
Purdue University, babbs@purdue.edu

Follow this and additional works at: http://docs.lib.purdue.edu/bmepubs

 Part of the Biomedical Engineering and Bioengineering Commons

Recommended Citation

Babbs, Charles F., "Optimizing Electrode Placement for Hemodynamic Benefit in Cardiac Resynchronization Therapy" (2012). *Weldon School of Biomedical Engineering Faculty Publications.* Paper 57.
http://docs.lib.purdue.edu/bmepubs/57

This document has been made available through Purdue e-Pubs, a service of the Purdue University Libraries. Please contact epubs@purdue.edu for additional information.

Optimizing Electrode Placement for Hemodynamic Benefit in Cardiac Resynchronization Therapy

CHARLES F BABBS, MD, PhD

Department of Basic Medical Sciences and Weldon School of Biomedical Engineering, Purdue University, West Lafayette, Indiana, USA

(PACE Volume 35, Issue 9, September 2012, Pages 1135–1145)
DOI: 10.1111/j.1540-8159.2012.03454.x

Abstract

Background: *Research is needed to explore the relative benefits of alternative electrode placements in biventricular and left ventricular pacing for heart failure with left bundle branch block (LBBB).*

Methods: *A fast computational model of the left ventricle, running on an ordinary laptop computer, was created to simulate the spread of electrical activation over the myocardial surface, together with the resulting electrocardiogram, segmental wall motion, stroke volume, and ejection fraction in the presence of varying degrees of mitral regurgitation. Arbitrary zones of scar and blocked electrical conduction could be modeled.*

Results: *Simulations showed there are both sweet spots and poor spots for left ventricular electrode placement, sometimes separated by only a few centimeters. In heart failure with LBBB pacing at poor spots can produce little benefit or even reduced pumping effectiveness. Pacing at sweet spots can produce up to 35% improvement in ejection fraction. Relatively larger benefit occurs in dilated hearts, in keeping with the greater disparity between early and late activated muscle. Sweet spots are typically located on the basal to mid-level, inferolateral wall. Poor spots are located on or near the interventricular septum. Anteroapical scar with conduction block causes little shift in locations for optimal pacing. Hearts with increased passive ventricular compliance and absence of pre-ejection mitral regurgitation exhibit greater therapeutic gain. The durations and wave shapes of QRS complexes in the electrocardiogram can help predict optimum electrode placement in real time.*

Conclusions: *Differences between poor responders and hyper-responders to cardiac resynchronization therapy can be understood in terms of basic anatomy, physiology, and pathophysiology. Computational modeling suggests general strategies for optimal electrode placement. In a given patient heart size, regional pathology, and regional dynamics allow individual pre-treatment planning to target optimal electrode placement.*

Key words: bundle-branch block, heart failure, mapping, mitral regurgitation

Introduction

Cardiac resynchronization therapy (CRT) involves atrio-leftventricular pacing or atrio-biventricular pacing in patients with complete heart block or left bundle branch block (LBBB)[1]. The atrial lead is placed high in the right atrium. The left ventricular lead is placed transvenously in a tributary of the coronary sinus[2] or implanted in an epicardial position at surgery[3]. In both left ventricular (LV) pacing and bi-ventricular (Bi-V) pacing ventricular stimulation is achieved by sensing intrinsic atrial activation signals to trigger AV-synchronous pacing. Bi-ventricular pacing frequently includes atrial pacing as well as atrial sensing. Left ventricular (LV) pacing is done using a shortened atrioventricular (AV) delay to pre-excite the left ventricle. The longest AV delay that still produces full pre-excitation is used. Bi-ventricular pacing is done by simultaneously activating the LV free wall and right ventricular apex via two ventricular leads. The target site for the right ventricular electrode is the right ventricular apex. The target site for the left ventricular electrode is typically the lateral or posterior wall, far from the right ventricular lead[4] in the case of Bi-V pacing.

The rationale for CRT is based on the high (30 to 50 percent) prevalence of intraventricular conduction delay among patients with heart failure[4]. In patients having heart failure and LBBB, early activated muscle can push on late activated muscle during the isovolumic contraction phase, stretching the opposing wall and causing paradoxical wall motion that is ineffective in generating aortic valve opening pressures or forward flow. In this way electrical delay translates into contractile dysfunction.[5] In addition late activation of the bases of the papillary muscles because of intraventricular conduction delay can lead to pre-ejection mitral regurgitation[6, 7].

In this setting CRT can resynchronize lateral and septal wall contraction to improve the function of the heart as a pump[6]. Indeed multiple clinical trials have established that in patients with severe heart failure (NYHA functional class III or IV, and LVEF <= 0.35) and intraventricular conduction delay (QRS complex duration > 120 to 150 msec) biventricular pacing increases the left ventricular ejection fraction, decreases mitral regurgitation, and improves symptoms caused by heart failure[4, 8-11]. An appealing aspect of CRT is that these acute hemodynamic benefits are achieved while reducing myocardial energy consumption[12]. The result is improved long term survival[13].

There is reasonable agreement that the left ventricular lead should be placed anatomically in a position close to the site of most delayed electromechanical activation[11]. Currently, echocardiography with tissue Doppler imaging can be performed in combination with electrophysiological measurements to determine the most delayed site of ventricular wall contraction[3, 4, 14]. However there are still non-responders, estimated to number between 25% and 30% of patients initially expected to benefit from CRT. Non-response may be due to local pathology, functional block, or less than optimal electrode placement[5]. Interestingly, there are also patients treated with CRT that have a “complete” recovery and have been labeled “hyper-responders” (about 13% of cases) who are usually patients with non-ischemic dilated cardiomyopathy[15]. This paper is dedicated to the proposition[16] that optimal electrode placement may further increase response probability over that achieved in current practice, decreasing the proportion of non-responders and improving overall success.

Short-term studies have suggested the lateral wall, midway between base and apex[3], as a reasonable target zone for left ventricular lead placement. Ariga and coworkers showed that greater three-dimensional ventricular lead tip separation is associated with improved outcome after cardiac resynchronization therapy[17]. However, recent echocardiographic studies suggest that in a substantial proportion of patients the anatomically selected pacing site does not always coincide with ventricular regions having large mechanical delay[11, 18]. Singh et al.[19] in a study of left ventricular lead position and clinical outcome (MADIT-CRT) found that leads positioned in the apical region were associated with an unfavorable outcome. Intuitively, myocardial fibrosis and heterogeneously dispersed scar and/or ischemia might easily modify how electrical delay translates into contractile dysfunction[5].

Accordingly, the objective of the present study was to create a computational model to help explain and predict (1) the linkage between electrical delay and decline in the function of the heart as a pump, (2) the roles heart failure, LBBB, pre-ejection mitral regurgitation, and patchy regional pathology in augmenting functional decline, and (3) the role of electrode placement in the efficacy of CRT. The aims were to refine general rules appropriate for most hearts and also to explore approaches for individualized treatment planning, incorporating available information such as on heart size, local pathology, 3D vector electrocardiography, and ultrasonic Doppler measurements of wall motion.

Methods

To study the relative benefits of alternative electrode placements in CRT a computer-based mathematical model of the left ventricle was created describing the spread of electrical activation over the myocardial surface and the resulting electrocardiogram, segmental wall motion, stroke volume, and ejection fraction. The model was implemented in Microsoft Visual Basic code within an Excel spreadsheet on an ordinary laptop computer and validated against known algebraic solutions for geometric shapes, electrocardiographic potentials in simple test cases, and expected regional wall motion in pathological cases.

Geometry

The left ventricular endocardium is modeled as a radially symmetrical, roughly bullet shaped surface, covered with a uniformly thick layer of cardiac muscle. The radius in the base-to-apex direction can be specified arbitrarily to model any degree of ventricular hypertrophy and dilatation. The muscle is capable of shortening proportionally in both radial and axial dimensions, in keeping with the generally helical wrapping of muscle fibers in a living heart[20, 21]. The muscle layer is divided into parallel slices perpendicular to the long axis of the left ventricle, as shown in Figure 1. Each slice has initial thickness, h, and is divided into a specified number of wedge shaped segments in the circumferential or hoop direction. The standard model has 6 slices of 12 segments each. For initial simulations the radial profile of the endocardial surface was a parabolic curve fit to a hand-drawn rendition of a typical left ventriculogram in diastole.

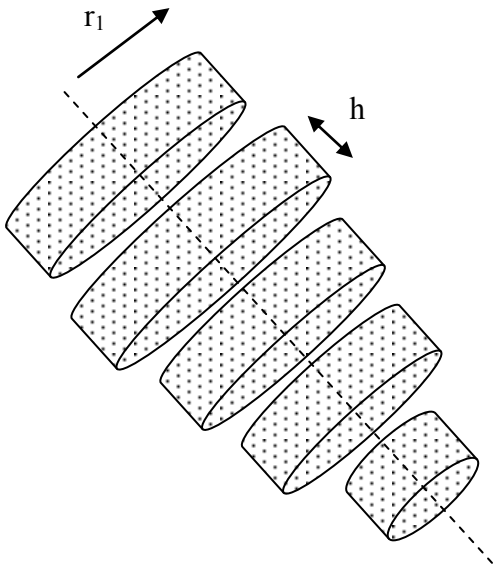

Figure 1. Exploded diagram of component longitudinal slices of the left ventricle. Radius r_1 of the first segment is shown.

Activation sequence

Propagation

Activation of the muscle in each segment occurs either by pacing at specified locations or by conduction from adjacent muscle at a constant conduction velocity (nominally 60 cm/sec[22, 23]). The activation sequence is described by a set of activation times, τ_{ij} , for each segment at radial position, i, and axial position, j, in the model. The center of each segment is called a node. Time zero indicates the onset of electrical ventricular stimulation in a cardiac cycle. To model LBBB time, τ_{ij} , is set to zero for right anterolateral segments in contact with distal fibers of the right bundle branch. For segments in contact with pacing electrodes, the time, τ_{ij} , represents the onset of pacing. For other segments activated by cell to cell conduction, the time, τ_{ij} , represents the time of arrival of the activation wave front at node (i, j).

The algorithm for tracking propagation of the wave of activation through the myocardium is as follows. Let k be an indexed node, and let n be a neighboring node in either the axial, diagonal, or radial direction. Let t be clock time, and let τ_n be the activation time of neighboring node, n. If node k is viable (not scar) but not yet active, and if node n is active, and if $t - \tau_n$ equals the impulse travel time between nodes k and n, then k becomes active with $\tau_k = t$. In this way the arrival of the activation wave front can be mapped as it spreads across the myocardium in terms of arrival times, τ_{ij}, for all nodes (i, j) in the model.

Activation display

To show a three dimensional movie of ventricular activation, an x,y,z coordinate system is defined for the chest with its origin at the base of the heart, the x-axis pointing to the left axilla, the y-axis pointing toward the feet, and the z-axis pointing anteriorly toward the sternum. Axial and radial coordinates for left ventricular nodes are computed and overlaid with the y-axis of the model. Then the axis of the left ventricle is rotated 30 degrees to the left and 30 degrees anteriorly to a more anatomically realistic orientation, using standard formulas for rotation of axes[24]. Locations of the endocardial nodes during activation are logged in this rotated x,y,z coordinate system. To create a movie of the activation sequence in time, t, ranging from 0 to t_{max} (when the last viable node is stimulated) all active nodes are displayed graphically in a frontal (x, y) projection every $1/40^{th}$ second of simulation time.

Dynamics

Active segments

Once the activation sequence and the set of times $\tau(i, j)$ have been computed and saved in memory, ventricular wall dynamics are found as follows. Left ventricular intracavitary volume is divided into wedge-shaped sections of local radius r_{ij} and local thickness h_{ij}, corresponding to each node of the model. After onset of activation these dimensions undergo shortening, representing cardiac muscle contraction. Muscle contraction lasts 40 percent of cycle time and has a half-sinusoidal waveform. In particular, the linear dimensions, r and h, are multiplied by a shortening factor $\phi_{ij}(t) = 1 - \max(0, \varepsilon_{max} \sin(2\pi(5/4)f(t - \tau_{ij})))$. Each local shortening factor $\phi_{ij}(t) \le 1$, has a half-sinusoidal waveform during systole and a constant value of 1 during diastole. The variable ε_{max} is the maximal shortening fraction for individual cardiomyocytes, and f is the pacing frequency in Hz. The duration of the positive half sinusoidal phase of function $\phi(t)$ is 40% of cycle time. For a normal ejection fraction of 60%, the maximal shortening, ε_{max}, would be
$1 - (0.4)^{1/3} = 0.26$, using classical scaling rules[25, 26].

Assuming each local intracavitary segment retains a wedge shape during systole that is geometrically similar to that in diastole, and using well-known scaling rules[25, 26] for similarly shaped objects, the local intracavitary volume at node (i, j) changes instantaneously as a function of time by a factor of $\phi_{ij}(t)^3$. Thus the sum of all volumes swept out by active muscle segments, $\Delta V_1(t)$, can be calculated easily for dynamic simulation time, t, ranging from 0 to t'_{max} (the end of ejection, when left ventricular volume is minimal).

Passive segments

Before opening of the aortic valve, the volume that is swept out by contraction of active segments distends the remaining passive segments. Let V_2 represent the instantaneous intracavitary volume underlying non-contracting muscle, scarred areas, and the mitral valve. The volumes underlying these passive surfaces are expanded by a factor of

$\Delta V_1(t) / V_2(t) = (\phi_2(t))^3$, where $\phi_2(t)$ is the extension ratio for the radius and height of the stretched, passive segments. For simplicity, the value of $\phi_2(t)$ is the same (an average value) for all passive segments. Thus before aortic valve opening, the remaining passive segments are stretched by factor of $\phi_2(t) = (\Delta V_1 / V_2)^{1/3}$ After aortic valve opening the amount of passive stretch of inactive or scarred segments is considered constant in time during ejection, as the left ventricle empties.

Left ventricular pressure

Left ventricular pressure before ejection is computed from the volume swept out by active muscle and the compliance of the remaining passive segments plus the compliance of the mitral valve in closed position. For initial end diastolic volume, V_0, of the left ventricle at time zero, the compliance of residual passive muscle and mitral valve together would be

$$C_p(t) = \frac{V_2(t)}{V_0} C_{pLV} = \frac{\Delta V_1(t)}{\Delta P(t)} ,$$

for instantaneous pressure rise, $\Delta P(t)$, in the left ventricle and passive compliance of the whole left ventricle with the mitral valve closed, C_{pLV}, which is a given model parameter. If the opening pressure in the aortic valve is $\Delta P_o \approx 80$ mmHg, then stretching of passive segments occurs either until the segments are activated and begin to contract or until

$$\Delta P(t) = \frac{V_0 \, \Delta V_1(t)}{C_{pLV} V_2(t)} > \Delta P_o \approx 80 \, \text{mmHg}$$

and the aortic valve opens, venting the left ventricular volume.

Left ventricular volume

Left ventricular volume is computed as the sum of all intracavitary volume wedges having local dimensions r_{ij} and h_{ij}. Stroke volume is computed as the difference between initial diastolic volume, V_0, and the minimum instantaneous left ventricular volume, minus any backward leaks through the mitral valve caused by papillary muscle dysfunction or frank mitral regurgitation.

Papillary muscle dysfunction and mitral regurgitation

Function of the papillary muscles and their dysfunction in complete heart block and left bundle branch block are modeled as follows. A fraction (ranging from zero to 40 percent) of the volume swept out by actively contracting muscle is allowed to leak from the left ventricular cavity until such time as the specified locations of the bases of the both the anterolateral and posteromedial papillary muscles are activated. This volume of retrograde leak is subtracted from the difference in end diastolic and end systolic intracavitary volumes to obtain forward stroke volume. In initial models mitral regurgitation was zero.

Regional pathology

Numerical entries in a table of all nodes are used to indicate areas of local scar or dysfunctional tissue. Both local impulse propagation velocity and local muscle contraction were set to zero in scared areas. Alternatively, slowed conduction or hypocontraction could be programmed, if desired.

Segmental wall motion

To show a three dimensional movie of ventricular wall dynamics in some simulations, the spatial locations of all endocardial nodes during activation and ejection were logged in the realistically rotated x,y,z coordinate system and the frontal (x, y) and lateral (y, z) projections displayed graphically to create movies of a wire frame model of the endocardium, similar to a left ventriculogram.

Simulation of the electrocardiogram

Coordinates, x,y,z, for the location of a typical "left arm" electrode were selected. To simulate the signal in lead aVL the summed dipole potential at this point, $U = \sum u_{ij}$, from all pairs of nodes in the model representing boundaries between active and passive muscle was computed versus the Wilson central terminal using the formula developed by Babbs[27],

$$u_{ij} = 3.5 \frac{A_{ij} \cos\theta_{ij}}{R_{ij}^2} \text{ millivolts}$$

for area, A_{ij}, of propagating wave front between nodes in either the axial or radial directions with left ventricular wall thickness equal to 1.5 cm from endocardium to epicardium; angle, θ_{ij}, between the axis of propagation and the line from the center of each dipole to the left arm electrode; and distance, R_{ij}, between the center of each dipole and the left arm electrode. As excitation spread outward from pacing sites around the myocardium in LBBB, the summed electrical potential, U, traced a simulated wide QRS complex based upon the array of electrical dipoles created at the interfaces between depolarized (contracting) and polarized (resting) muscle tissue[27]. Simulated scar tissue did not contribute to electrical potentials.

Parameter values

Required numerical values for a standard, normal sized heart model are summarized in Table 1. The standard model included 72 nodes (12 radial x 6 axial) representing the left ventricular endocardium and overlying muscle. Spread of the wave front of activation was computed every 0.2 msec. The heart rate was 80 beats per minute and the duration of systole was 40 percent of cycle time. Passive left ventricular compliance was estimated as ~ 1 ml/mmHg by dividing typical normal values for left atrial pressure rise and left ventricular volume increase during atrial contraction in sinus rhythm.

TABLE 1. Parameter Values for Primary Model.*

Parameter	Numerical value	Units
Base to apex dimension	9	cm
Maximal LV radius	2.7	cm
Number of nodes in hoop dimensions	12	
Number of nodes in axial dimension	6	
Muscle to muscle impulse conduction velocity	60	cm/sec
Passive LV compliance	1	ml/mmHg
Fraction of LV volume underlying non-muscle tissue	0.15	
Heart rate	80	1/min
Diastolic arterial pressure	80	mmHg
LV axis with respect to vertical and horizontal	30	degrees

* LV denotes left ventricle; normal heart size (scale = 1.0)

In the primary model for a normal sized heart the radius, r, in centimeters was defined as $r = 2 + 0.65n - 0.15n^2$ for node number, n, in the axial dimension, measured from the base of the heart toward the apex. Thus, the internal radii of the six transverse slices of left ventricular myocardium were 2.5, 2.7, 2.6, 2.2, 1.5, and 0.5 cm, respectively. In the primary model for a dilated heart the linear dimensions of the internal radii and the axial slice separation, h, were multiplied by a factor of 1.5. In turn, end diastolic volume increased from 130 to 440 ml. The base of the anterolateral papillary muscle was located approximately 54 degrees to the left of anterior and 60 percent of the distance from base to apex. The base of the posteromedial papillary muscle was located approximately 144 degrees to the right of anterior and 50 percent of the distance from base to apex.

Heart failure with left bundle branch block

Left bundle branch block with left ventricular pacing was simulated in two models of heart failure. The first had uniform reduction in muscle contraction throughout the left ventricle (nonischemic cardiomyopathy). The second had an anteroapical region of scar tissue that did not conduct or contract in the territory of the left anterior descending coronary artery (old apical infarct in the setting of ischemic heart disease).

Heart failure was simulated by adjusting maximal fiber shortening, e_{max}, of normal muscle so that ejection fraction was < 35%, representing patients who would be legitimate candidates for bi-ventricular pacing. The maximal linear shortening of muscle fibers in the normal sized heart model was 0.15, creating a control stroke volume of 33 ml and an ejection fraction of 25%. The maximal linear shortening of muscle fibers in the 1.5x dilated heart model was 0.075, creating a control stroke volume of 47 ml and an ejection fraction of 11%.

Ventricular beats with LBBB were initiated along the apical half of the meridian stretching from the right ventricular apex to the interventricular septum, at an angle approximately 45 degrees counterclockwise from the vertical (anterior) position on the left ventricular profile. This location corresponds to the branched distal half of the right bundle branch, which would stimulate the interventricular septum to produce a pattern of ventricular breakthrough and activation similar to that reported in the literature[23, 28]. After time zero, activation spreads outward by cell to cell conduction.

Left ventricular versus bi-ventricular pacing

To simulate the LV pacing mode with pre-excitation of the left ventricle the site of the left ventricular electrode is activated at time zero. Subsequent excitation of the interventricular septum by the intact right bundle branch block is modeled the same way as in untreated LBBB, beginning after a delay of 50 msec. This delay represents the difference between the normal AV conduction time (150 msec) and the programmed pre-excitation delay (100 msec). To simulate biventricular pacing, both the left ventricular pacing site and a right ventricular apical pacing site are activated simultaneously at time zero. Thus in both modes time zero represents the earliest onset of ventricular excitation. (Atrial pacing and pumping are not included for simplicity.) Unless otherwise specified, the location of the right ventricular electrode for Bi-V pacing was on the anterolateral interventricular septum, 75% of the distance from base to apex.

Results

Simulated biventricular and left ventricular pacing in heart failure with LBBB

The figure of merit to assess the benefit or harm of CRT was the percentage change in stroke volume, compared with native LBBB, caused by left ventricular pacing at any specified location. Figure 2 shows endocardial maps of the percentage change in stroke volume obtained when bi-ventricular pacing was initiated at any particular LV site together with an electrode at the right ventricular apex. The perspective shown is that obtained by opening the left ventricle by an

anterior longitudinal incision from base to apex (about 1 cm left of the left anterior descending coronary artery) and separating the halves of the left ventricle laterally in a clamshell configuration. The base of the heart is shown toward the top and the apex toward the bottom. The interventricular septum is anatomically on the right (left hand side of the drawing). The left ventricular free wall is anatomically on the left (right hand side of the drawing), and the posterior ventricular wall is in the middle.

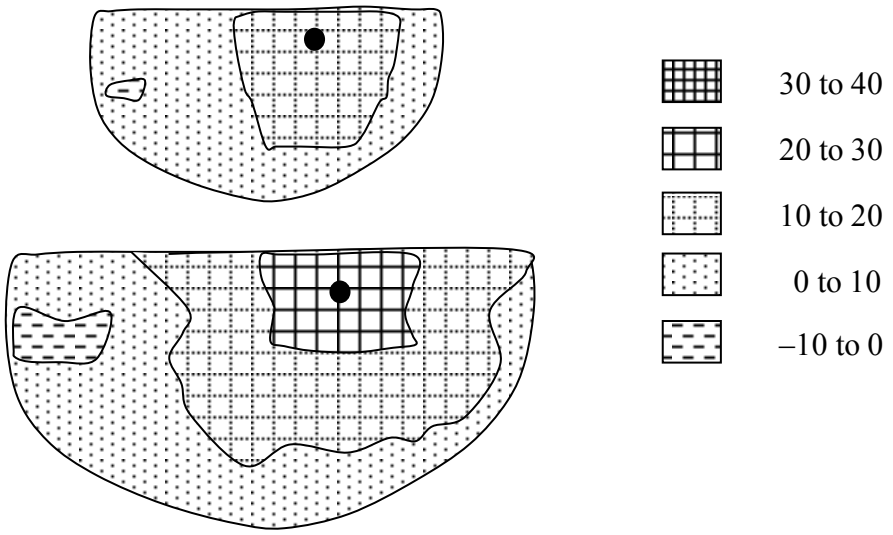

Figure 2. Percentage changes in stroke volume with bi-ventricular pacing at various locations mapped onto the surface of the left ventricular endocardium in models of heart failure plus LBBB. Map indicates sites of the left ventricular electrode. Normal sized heart on top; 1.5x enlarged heart on bottom. Solid dot indicates optimum placement.

Stroke volume is diminished by bi-ventricular pacing in the region of the mid-interventricular septum, causing a negative change. Stroke volume is augmented by bi-ventricular pacing in the basilar region of the posterolateral wall, causing a positive change. There are both sweet spots and sour spots for biventricular pacing. The magnitudes of the changes range from –1% to 17% in normal sized hearts (above) and from –3% to 24% in dilated hearts. As expected, simulated cineangiograms of LBBB (not shown) indicate paradoxical budging in late-activated muscle. Bi-ventricular pacing near this late activated site produces the greatest improvement in stroke volume. Black dots indicate pacing sites for maximal gain in stroke volume. Cross-hatched shading indicates larger target zones for electrode placement with similarly positive hemodynamic benefit. Such nearly optimal regions for left ventricular electrode placement may be practically achievable.

Figure 3 shows endocardial maps obtained when left-ventricular pacing was initiated in models of heart failure with LBBB assuming a 100 msec AV delay and a 150 msec natural AV conduction time. Hence the LV pacing site was activated by LV pacing 50 msec before the right anteroapical interventricular septum was activated by the intact right bundle branch. The positive effects of pacing of the left ventricular free wall are similar to those in bi-ventricular pacing. The relative improvement of stroke volume ranged from –8% to 19% in normal sized hearts and from –5% to 35% in enlarged hearts. Optimal LV pacing sites are somewhat closer to the cardiac apex than in bi-ventricular pacing. Pacing of the interventricular septum or adjacent regions produces little or no benefit and occasionally some harm.

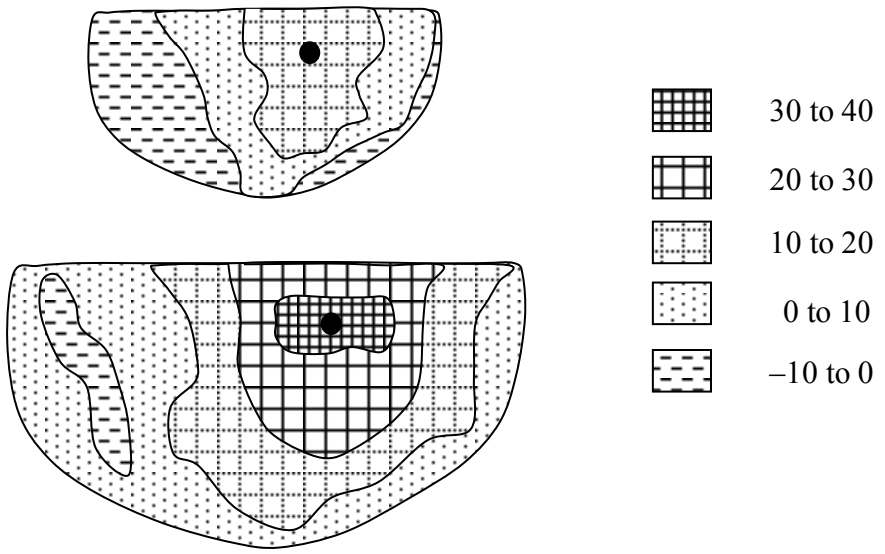

Figure 3. Percentage changes in stroke volume at various locations with left-ventricular pacing and pre-excitation of the left ventricle 50 msec before activation of anteroapical muscle by the native right bundle. Other details similar to Figure 2.

Right ventricular electrode placement

The benefit of Bi-V pacing depends on the position of the right ventricular pacing electrode as well as the left ventricular electrode. In Figure 2 the RV electrode was located at a position along the interventricular septum corresponding to the latitude of the right ventricular apex, three quarters of the distance from the left ventricular base to the left ventricular apex. Other locations for the septal electrode are shown in Figure 4 in terms of the percentage distance from base to apex along the septum, including one extreme apical position that would require epicardial rather than transvenous electrode placement. Left ventricular electrode placement was constant at a position corresponding to the optimal location in Figure 2 (posterolateral base). The dashed line indicates the improvement in ejection fraction with LV pacing. The dotted line indicates the

improvement in ejection fraction of with an idealized Purkinje system that achieves simultaneous activation of all ventricular muscle at time zero.

There are only modest differences in acute hemodynamic effectiveness between LV and Bi-V pacing when the right ventricular electrode pacing electrode is located near the mid portion of the interventricular septum. A modest improvement over the right ventricular apical position may be possible with electrode positions higher up on the septal wall.

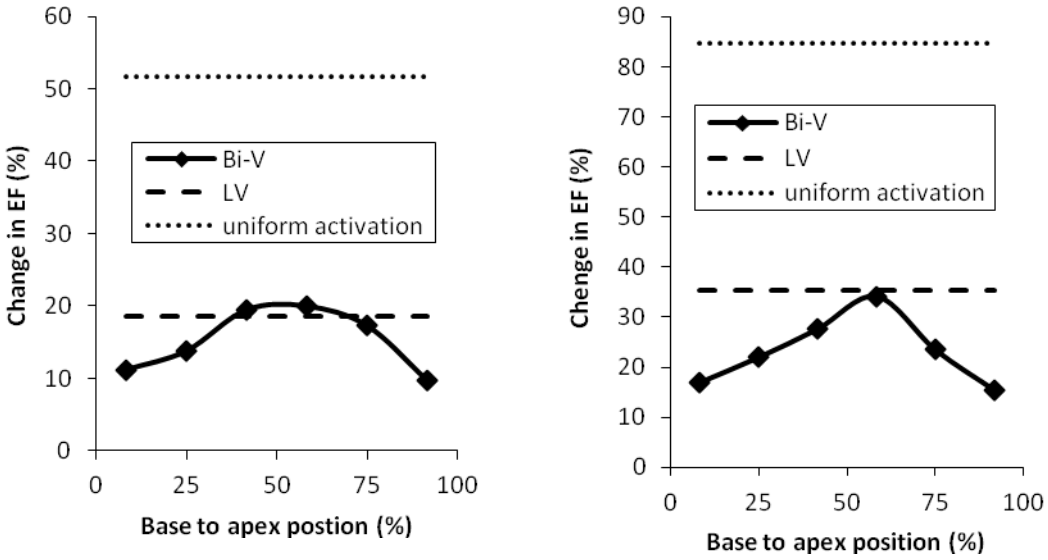

Figure 4. Percentage changes in ejection fraction for bi-ventricular pacing with variable positions of the septal electrode in models of heart failure with LBBB. Left ventricular electrode position was constant at node location 8,1. Normal sized heart on left, dilated heart on right. Note differences in the vertical scales.

Passive left ventricular compliance

In keeping with the mechanistic hypothesis that paradoxical bulging of late activated muscle is the root cause of stroke volume loss in heart failure with LBBB, the author explored effects of varying passive LV compliance. Figure 5 shows the dependence of stroke volume on passive ventricular compliance of with native LBBB and during electrode position optimized Bi-V pacing on for the normal sized and dilated heart models. Increased passive compliance worsens stroke volume with native LBBB and allows for relatively greater therapeutic gain from Bi-V pacing.

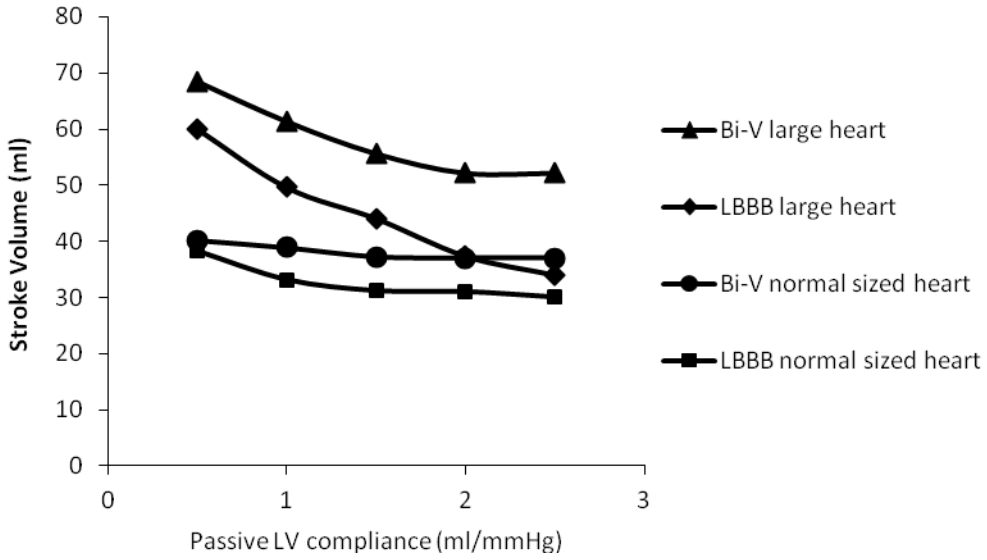

Figure 5. Computed stroke volumes for heart failure and native LBBB versus bi-ventricular pacing with variable passive left ventricular compliance.

Pre-ejection mitral regurgitation

Figure 6 shows the benefits of electrode position optimized Bi-V pacing in patients with varying degrees of pre-ejection mitral regurgitation. In these models a varying fraction, shown on the horizontal axis, of the volume swept out by contracting muscle flowed retrograde until 10 msec after the bases of both anterior and posterior papillary muscles in the left ventricle were activated. These models recreated varying degrees of LBBB induced pre-ejection papillary muscle dysfunction. Increasing pre-ejection mitral regurgitation degrades the therapeutic gain of bi-ventricular pacing.

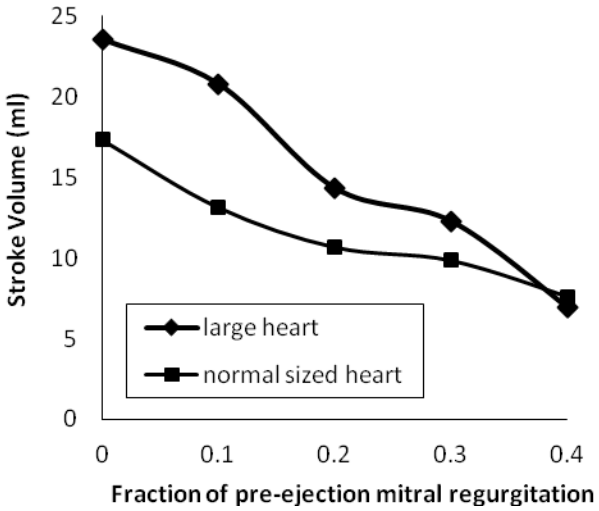

Figure 6. Computed percentage improvement in stroke volume for bi-ventricular pacing with optimized LV electrode placement and variable degrees of early pre-ejection mitral regurgitation.

Simulated biventricular pacing in heart failure, LBBB, and local apical pathology

The effects of anteroapical scar were simulated by blocking impulse activation, impulse conduction, and muscle contraction in the scarred region. Scarred tissue had passive compliance properties. These simulations represented extreme local pathology located in the distribution of the left anterior descending coronary artery. Maps of hemodynamic effectiveness vs. LV electrode placement like those in Figure 2 were constructed for the local scar models. Percentage changes in ejection fraction were similar to non-scarred models, ranging from –5% to 13% for the normal sized heart model (compared with–1% to 17% in models without regional pathology) and from –17% to 21% in scarred and dilated heart models (compared with –3% to 24% in models without regional pathology). Local pathology slightly increases the downside and reduces the upside of CRT. There are also small shifts in the positions of optimal LV electrode placements toward the sites of scar (Figure 7). Importantly, local pathology appears to increase the sizes of zones associated with negative hemodynamic benefit.

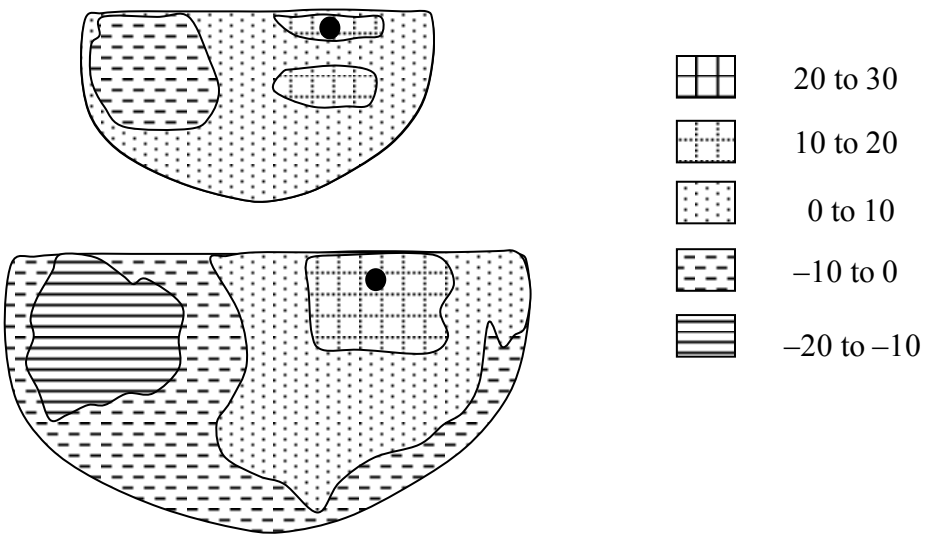

Figure 7. Percentage changes in stroke volume with bi-ventricular pacing at various locations mapped onto the surface of the left ventricular endocardium in models of heart failure, LBBB, and scared anteroapical ventricular muscle. Other details similar to Figure 2.

Simulated electrocardiographic waveforms as guides to electrode placement

Figure 8 shows the simulated electrocardiographic waveforms of QRS complexes in Lead aVL for native LBBB (curve 1, dotted line) and for optimal biventricular pacing (curve 2, solid line) in the model of complete heart block. Optimal biventricular pacing shortens the duration and reduces the voltage of the paced QRS complex, producing a characteristic low-amplitude, "isoelectric" waveform pattern in Lead aVL.

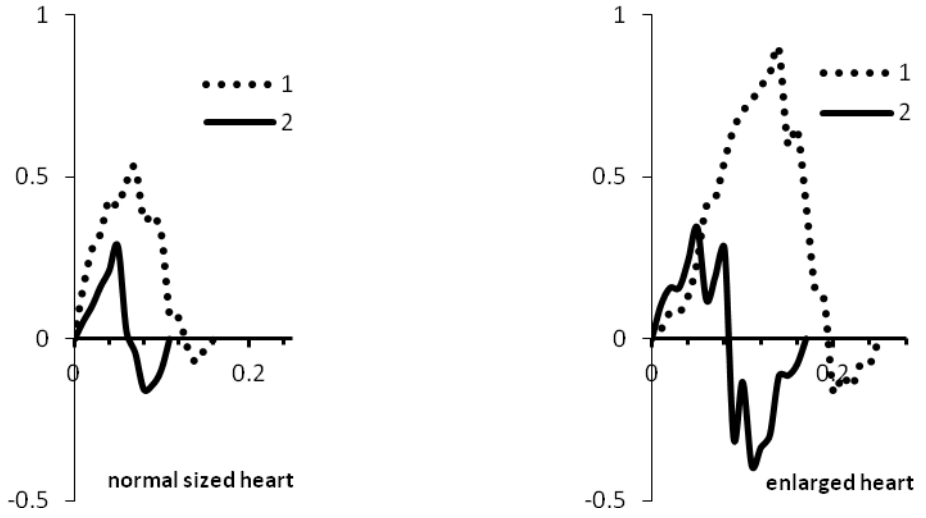

Figure 8. Simulated QRS complexes in lead aVL for model of heart failure plus LBBB. Curve 1 represents native LBBB. Curve 2 represents bi-ventricular pacing at the optimal posterolateral electrode location. Pacing spikes are not shown. Voltage scales are in millivolts. Time scales are in seconds.

Discussion

Location of the left ventricular pacing electrode is critical for hemodynamic benefit in CRT. There are sweet spots that substantially improve pumping and also sour spots that may actually reduce forward flow. In between there are regions of little therapeutic benefit. Previous authors have described poor responders and hyper-responders[15] to CRT. The importance of placing the second pacing electrode far from the first has also been recognized[17]. This modeling study extends and confirms these empirical findings and shows that they can be understood in terms of basic anatomy and physiology. In the absence of a working Purkinje system, dual pacing sites on opposite sides of the left ventricle allow for more nearly simultaneous activation, providing a first level of validation of the model based on available published data.

Mathematical models can help explain and predict the variable results of CRT and can aid in treatment planning. The models presented here can be readily expanded to include arbitrarily shaped geographic areas of scar tissue or ischemia with variably decreased cell to cell conduction velocity and local contractile shortening. Using available clinical data suggesting the type and location of myocardial pathology, heart size, and diastolic blood pressure, and the presence of any mitral regurgitation, one can create patient individualized models for treatment planning that

predict not only the zones of maximal benefit, but also the morphology of paced QRS complexes in any electrocardiographic lead. These might well be used to help identify proper electrode placement in real time, since the paced QRS waveform and duration may give an immediate indication, during the implant procedure, of effectiveness in any given patient. In this way model-based treatment planning could be a significant aid to navigation in this tricky clinical environment.

Results generated by the present computational models are consistent with earlier clinical observations in terms of the predicted patterns of activation, the predicted reduction in QRS complex duration, and the predicted improvement in pumping effectiveness.

Patterns of activation and contraction

The sequences of electrical activation and the patterns of wall motion predicted by the model are realistic and similar to those described by Auricchio and Abraham[29] and by Fung and Berger et al.[23, 28] Activation travels essentially in circumferential directions, justifying the one layer muscle model. As expected, left bundle branch block results in delayed depolarization and contraction of the left ventricular free wall, accompanied by early paradoxical bulging.

QRS duration reduction

Changes in QRS duration produced by CRT, as predicted by the model, are also in reasonable agreement with published studies, which found mean reductions in QRS complex duration from 182 to 143 msec[3], 174 to 157 msec[4], and 190 to 165 msec[30]. Simulations of Figure 8 show comparable reductions in QRS durations.

Improved pumping

The present computational models predict the improvements in the function of the heart as a pump produced by CRT with posterolateral free wall placement of the left ventricular pacing electrode in the range of –10 to +35 percent. Clinical studies show similar results in terms of mean values in small series of patients: 16%[31] and 18%[32] improvement in pulse pressure, 12% improvement in ejection fraction[7], and 48% increase in ejection fraction at 1 year follow up.[33] (Note in comparing one year follow up data, the present model does not include late effects such as reverse remodeling or improved myocardial metabolism associated with earlier relaxation and longer perfusion time, however, the model does include redistribution of regional ventricular loading, and reduction or abolition of mitral regurgitation.) The calculated rough equivalence of acute hemodynamic benefits of LV and Bi-V pacing agrees with the rough equivalence of long term benefit reported by Thibault and coworkers[34]. Modeling predicts a range of potential benefit within the general posterolateral wall area, offering the promise of better results with better targeting of electrode placement. However, non-response remains a distinct possibility with poor electrode placement and smaller heart size.

The present modeling approach is limited to the effects of defined inputs. The intent is to capture the essence of underlying mechanisms with reasonable mathematical simplicity. However, it is quite possible that unmodeled variables or confounders might be present in some

patients that would influence results. For example, the present model includes only a single layer of cardiac muscle, rather than multiple layers from endocardium to epicardium. Multiple layers of myocardium, which can be added to the model at the cost of some complexity and increased computation time, might make a biologically meaningful difference in cases of left ventricular hypertrophy, much more than in cases of dilated cardiomyopathy where the wall thickness dimension is less prominent. Also, the present model is intended to predict acute hemodynamic gain only and does not reflect effects of tissue remodeling. As such it might underestimate the long term benefits of CRT.

Conclusions

The present simple and easily implemented computational models can inform targeting of left ventricular electrode placement in a general way and even allow for patient individualized treatment planning in the presence of variable left ventricular activation patterns[28] and pathologies. Identifying a particular patient's sweet spot in a process of computer aided individual treatment planning should be possible using models that receive multi-modal input regarding the size and local pathology of a particular heart, including regional wall motion by echocardiography[35, 36]. Such methods for better definition of optimal electrode placement may guide clinicians using the transvenous approach or perhaps suggest alternative open surgical[3] or percutaneous transapical approaches[37], if coronary sinus and cardiac vein anatomy are unfavorable for transvenous techniques.

References

1. Vardas PE, Auricchio A, Blanc JJ, Daubert JC, Drexler H, Ector H, Gasparini M, Linde C, Morgado FB, Oto A, Sutton R, Trusz-Gluza M. Guidelines for cardiac pacing and cardiac resynchronization therapy: The task force for cardiac pacing and cardiac resynchronization therapy of the european society of cardiology. Developed in collaboration with the european heart rhythm association. *European heart journal*. 2007;28:2256-2295
2. Daubert JC, Ritter P, Le Breton H, Gras D, Leclercq C, Lazarus A, Mugica J, Mabo P, Cazeau S. Permanent left ventricular pacing with transvenous leads inserted into the coronary veins. *Pacing Clin Electrophysiol*. 1998;21:239-245
3. Mair H, Sachweh J, Meuris B, Nollert G, Schmoeckel M, Schuetz A, Reichart B, Daebritz S. Surgical epicardial left ventricular lead versus coronary sinus lead placement in biventricular pacing. *Eur J Cardiothorac Surg*. 2005;27:235-242
4. Cazeau S, Leclercq C, Lavergne T, Walker S, Varma C, Linde C, Garrigue S, Kappenberger L, Haywood GA, Santini M, Bailleul C, Daubert JC. Effects of multisite biventricular pacing in patients with heart failure and intraventricular conduction delay. *N Engl J Med*. 2001;344:873-880
5. Kass DA. Cardiac resynchronization therapy. *Journal of cardiovascular electrophysiology*. 2005;16 Suppl 1:S35-41
6. Kanzaki H, Bazaz R, Schwartzman D, Dohi K, Sade LE, Gorcsan J, 3rd. A mechanism for immediate reduction in mitral regurgitation after cardiac resynchronization therapy:

Insights from mechanical activation strain mapping. *J Am Coll Cardiol*. 2004;44:1619-1625
7. Etienne Y, Mansourati J, Touiza A, Gilard M, Bertault-Valls V, Guillo P, Boschat J, Blanc JJ. Evaluation of left ventricular function and mitral regurgitation during left ventricular-based pacing in patients with heart failure. *European journal of heart failure*. 2001;3:441-447
8. Bradley DJ, Bradley EA, Baughman KL, Berger RD, Calkins H, Goodman SN, Kass DA, Powe NR. Cardiac resynchronization and death from progressive heart failure: A meta-analysis of randomized controlled trials. *Jama*. 2003;289:730-740
9. Hunt SA, Abraham WT, Chin MH, Feldman AM, Francis GS, Ganiats TG, Jessup M, Konstam MA, Mancini DM, Michl K, Oates JA, Rahko PS, Silver MA, Stevenson LW, Yancy CW, Antman EM, Smith SC, Jr., Adams CD, Anderson JL, Faxon DP, Fuster V, Halperin JL, Hiratzka LF, Jacobs AK, Nishimura R, Ornato JP, Page RL, Riegel B. Acc/aha 2005 guideline update for the diagnosis and management of chronic heart failure in the adult: A report of the american college of cardiology/american heart association task force on practice guidelines (writing committee to update the 2001 guidelines for the evaluation and management of heart failure): Developed in collaboration with the american college of chest physicians and the international society for heart and lung transplantation: Endorsed by the heart rhythm society. *Circulation*. 2005;112:e154-235
10. Strickberger SA, Conti J, Daoud EG, Havranek E, Mehra MR, Pina IL, Young J. Patient selection for cardiac resynchronization therapy: From the council on clinical cardiology subcommittee on electrocardiography and arrhythmias and the quality of care and outcomes research interdisciplinary working group, in collaboration with the heart rhythm society. *Circulation*. 2005;111:2146-2150
11. Ansalone G, Giannantoni P, Ricci R, Trambaiolo P, Fedele F, Santini M. Biventricular pacing in heart failure: Back to basics in the pathophysiology of left bundle branch block to reduce the number of nonresponders. *Am J Cardiol*. 2003;91:55F-61F
12. Nelson GS, Berger RD, Fetics BJ, Talbot M, Spinelli JC, Hare JM, Kass DA. Left ventricular or biventricular pacing improves cardiac function at diminished energy cost in patients with dilated cardiomyopathy and left bundle-branch block. *Circulation*. 2000;102:3053-3059
13. Rivero-Ayerza M, Theuns DA, Garcia-Garcia HM, Boersma E, Simoons M, Jordaens LJ. Effects of cardiac resynchronization therapy on overall mortality and mode of death: A meta-analysis of randomized controlled trials. *European heart journal*. 2006;27:2682-2688
14. Bax JJ, Ansalone G, Breithardt OA, Derumeaux G, Leclercq C, Schalij MJ, Sogaard P, St John Sutton M, Nihoyannopoulos P. Echocardiographic evaluation of cardiac resynchronization therapy: Ready for routine clinical use? A critical appraisal. *J Am Coll Cardiol*. 2004;44:1-9
15. Castellant P, Fatemi M, Bertault-Valls V, Etienne Y, Blanc JJ. Cardiac resynchronization therapy: "Nonresponders" And "Hyperresponders". *Heart Rhythm*. 2008;5:193-197
16. Auricchio A, Klein H, Tockman B, Sack S, Stellbrink C, Neuzner J, Kramer A, Ding J, Pochet T, Maarse A, Spinelli J. Transvenous biventricular pacing for heart failure: Can the obstacles be overcome? *Am J Cardiol*. 1999;83:136D-142D

17. Ariga R, Tayebjee MH, Benfield A, Todd M, Lefroy DC. Greater three-dimensional ventricular lead tip separation is associated with improved outcome after cardiac resynchronization therapy. *Pacing Clin Electrophysiol*. 2010;33:1490-1496
18. Auricchio A, Fantoni C, Regoli F, Carbucicchio C, Goette A, Geller C, Kloss M, Klein H. Characterization of left ventricular activation in patients with heart failure and left bundle-branch block. *Circulation*. 2004;109:1133-1139
19. Singh JP, Klein HU, Huang DT, Reek S, Kuniss M, Quesada A, Barsheshet A, Cannom D, Goldenberg I, McNitt S, Daubert JP, Zareba W, Moss AJ. Left ventricular lead position and clinical outcome in the multicenter automatic defibrillator implantation trial-cardiac resynchronization therapy (madit-crt) trial. *Circulation*. 2011;123:1159-1166
20. Buckberg GD, Clemente C, Cox JL, Coghlan HC, Castella M, Torrent-Guasp F, Gharib M. The structure and function of the helical heart and its buttress wrapping. Iv. Concepts of dynamic function from the normal macroscopic helical structure. *Seminars in thoracic and cardiovascular surgery*. 2001;13:342-357
21. Buckberg GD, Coghlan HC, Torrent-Guasp F. The structure and function of the helical heart and its buttress wrapping. Vi. Geometric concepts of heart failure and use for structural correction. *Seminars in thoracic and cardiovascular surgery*. 2001;13:386-401
22. Rohr S. Role of gap junctions in the propagation of the cardiac action potential. *Cardiovasc Res*. 2004;62:309-322
23. Berger T, Pfeifer B, Hanser FF, Hintringer F, Fischer G, Netzer M, Trieb T, Stuehlinger M, Dichtl W, Baumgartner C, Pachinger O, Seger M. Single-beat noninvasive imaging of ventricular endocardial and epicardial activation in patients undergoing crt. *PloS one*. 2011;6:e16255
24. Grossman SI. *Calculus*. New York: Academic Press; 1981.
25. Brown JH, West GB, Enquist BJ. Scaling in biology: Patterns and processes, causes and consequences. In: Brown JH, West GB, eds. *Scaling in biology*. New York: Oxford University Press; 2000:1-9.
26. Schmidt-Nielsen K. *Scaling: Why is animal size so important?* Cambridge: Cambridge University Press; 1984.
27. Babbs CF. Quantitative prediction of body surface potentials from myocardial action potentials using a summed dipole model. *Cardiovascular engineering (Dordrecht, Netherlands)*. 2009;9:59-71
28. Fung JW, Yu CM, Yip G, Zhang Y, Chan H, Kum CC, Sanderson JE. Variable left ventricular activation pattern in patients with heart failure and left bundle branch block. *Heart (British Cardiac Society)*. 2004;90:17-19
29. Auricchio A, Abraham WT. Cardiac resynchronization therapy: Current state of the art: Cost versus benefit. *Circulation*. 2004;109:300-307
30. Horwich T, Foster E, De Marco T, Tseng Z, Saxon L. Effects of resynchronization therapy on cardiac function in pacemaker patients "Upgraded" To biventricular devices. *Journal of cardiovascular electrophysiology*. 2004;15:1284-1289
31. Nelson GS, Curry CW, Wyman BT, Kramer A, Declerck J, Talbot M, Douglas MR, Berger RD, McVeigh ER, Kass DA. Predictors of systolic augmentation from left ventricular preexcitation in patients with dilated cardiomyopathy and intraventricular conduction delay. *Circulation*. 2000;101:2703-2709

32. Kass DA, Chen CH, Curry C, Talbot M, Berger R, Fetics B, Nevo E. Improved left ventricular mechanics from acute vdd pacing in patients with dilated cardiomyopathy and ventricular conduction delay. *Circulation*. 1999;99:1567-1573
33. Capasso F, Giunta A, Stabile G, Turco P, La Rocca V, Grimaldi G, De Simone A. Left ventricular functional recovery during cardiac resynchronization therapy: Predictive role of asynchrony measured by strain rate analysis. *Pacing Clin Electrophysiol*. 2005;28 Suppl 1:S1-4
34. Thibault B, Ducharme A, Harel F, White M, O'Meara E, Guertin MC, Lavoie J, Frasure-Smith N, Dubuc M, Guerra P, Macle L, Rivard L, Roy D, Talajic M, Khairy P. Left ventricular versus simultaneous biventricular pacing in patients with heart failure and a qrs complex >/=120 milliseconds. *Circulation*.124:2874-2881
35. Mullens W, Tang WH, Grimm RA. Using echocardiography in cardiac resynchronization therapy. *American heart journal*. 2007;154:1011-1020
36. Sanderson JE. Echocardiography for cardiac resynchronization therapy selection: Fatally flawed or misjudged? *J Am Coll Cardiol*. 2009;53:1960-1964
37. Kassai I, Friedrich O, Ratnatunga C, Betts TR, Mihalcz A, Szili-Torok T. Feasibility of percutaneous implantation of transapical endocardial left ventricular pacing electrode for cardiac resynchronization therapy. *Europace*. 2011;13:1653-1657